Shear Modulus and Plasticity of a Driven Charge Density Wave

A. F. Isakovic,[1] P. G. Evans,[2] J. Kmetko,[1] K. Cicak,[1,†] Z. Cai,[3] B. Lai,[3] and R. E. Thorne[1,*]

[1]*Laboratory of Atomic and Solid State Physics, Cornell University, Ithaca, New York 14853, USA*

[2]*Department of Materials Science and Engineering, University of Wisconsin, Madison, Wisconsin 53706, USA*

[3]*Advanced Photon Source, Argonne National Laboratory, Argonne, Illinois 60439, USA*

(Received 12 August 2005; published 30 January 2006)

We have probed the effects of transverse variations in pinning strength on charge-density-wave (CDW) structure in $NbSe_3$ by x-ray micro-beam diffraction. In ribbonlike crystals having a large longitudinal step in thickness, the CDW first depins on the thick side of the step, causing rotations of the CDW wave vector. By measuring these rotations as a function of position and electric field, the corresponding shear strains are determined, allowing the CDW's shear modulus to be estimated. These results demonstrate the usefulness of x-ray microdiffraction as a tool in studying collective dynamics in electronic crystals.

DOI: 10.1103/PhysRevLett.96.046401 PACS numbers: 71.45.Lr, 61.72.Dd, 68.37.−d

The structure and dynamics of charge (or spin) density waves in quasi-one-dimensional conductors illuminates the physics of single-particle and collective interactions in the presence of quenched and thermal disorder [1–3], and can provide insight into related systems including charge or spin striped phases [4], Wigner crystals [5], and moving flux line lattices [6]. Impurities and other defects pin the charge-density wave (CDW), so that an electric field greater than a threshold field E_T must be applied to produce steady motion. The elastic properties of CDWs provide a basis for understanding the structure of the pinned state, the character of the depinning transition, and the remarkable sliding dynamics that occur above it.

CDW plasticity strongly modifies measured properties, and is interdependent with fundamental electronic and optical properties [1,2]. For crystal thicknesses less than 10 μm, typical of CDW conductors including $NbSe_3$ and TaS_3, the depinning field increases with decreasing thickness [7]. These crystals almost always exhibit steps in thickness running along their length, as shown in Fig. 1, resulting in nonuniform pinning across their width. The thicker, more weakly pinned side may then shear from the thinner side at the measured E_T, as has been observed by x-ray topography [8], resulting in enormous $1/f$-like noise [9], loss of CDW coherence, and strong modifications to the velocity-field relation.

Here we report x-ray micro-beam diffraction measurements of the CDW shear strain profile induced by applied electric fields in stepped $NbSe_3$ crystals. Shear strains are largest near the step, and show a maximum just above E_T before decreasing at higher fields. From these measurements, we are able to determine the CDW's shear modulus. In the field of electronic crystals, artificially created nonuniform pinning has been used to determine shear elastic moduli of flux line lattices [6].

$NbSe_3$ crystals were selected that had a single large step running along their $\boldsymbol{b}^*$ axis, as shown schematically in Fig. 1(a). We present here data here for two of these samples, A and B, with widths of 15 μm and 12 μm and average thicknesses of 1.2 μm and 1.4 μm, respectively. Figure 1(b) shows an atomic force microscopy scan of the thickness step on crystal *A*, having a height of 0.7 μm. The

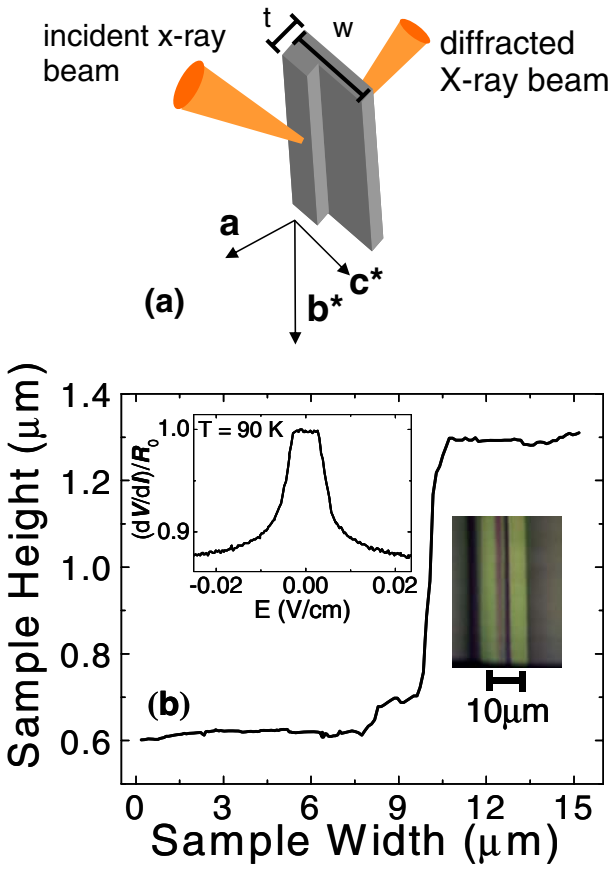

FIG. 1 (color online). (a) X-ray micro-beam setup for a $NbSe_3$ crystal with a stepped cross section, showing the relevant crystallographic directions. Momentum transfer is along the CDW transport direction ($\boldsymbol{b}^*$). (b) AFM profile of the stepped sample A used in this study. Right inset: optical image of sample A. Left inset: differential resistance vs electric field E for sample A at $T = 90$ K.

resulting thickness ratio produces a depinning field in the thin side roughly double that in the thick side, with the latter determining the measured E_T. Although crystals can have several much smaller steps, transport measurements [10] indicate that the single large step dominates the shear behavior.

Crystals were placed on 60 μm thick, x-ray transparent silicon substrates patterned with four gold electrical contacts, and then fixed to the substrate using a thin polymer film. The right inset of Fig. 1(b) shows an optical image of sample A mounted on the substrate. Samples were wired into an open-cycle He cryostat having an x-ray transparent beryllium window. The cryostat was mounted in a six-circle diffractometer.

X-ray micro-beam diffraction has been used to study dynamics in systems with structure on the mesoscale, including domain switching in spin wave systems and other strongly correlated compounds [11,12]. The present experiments were performed using the microdiffraction facility at beamline 2-ID-D at the Advanced Photon Source [13]. The submicron spatial resolution of x-ray microdiffraction is an excellent match for the predicted length scale of the CDW shear process, of the order of 1 μm, which has not been accessible in previous x-ray diffraction experiments.

10 keV x rays selected by a double bounce Si(111) monochromator were focused using a Fresnel zone plate and a 30 μm order-sorting aperture. The zone plate focusing optics introduced a beam divergence at the sample of 0.050°. We are able to determine the center of the intensity distribution with much higher accuracy than the divergence, and could resolve rotations of the CDW wave vector as small as 0.005° [8,11]. Diffracted x rays were collected using a photon-counting detector. By raster scanning the sample relative to the zone plate with the diffraction condition set for a fixed scattered wave vector, we collected spatial maps similar to those acquired using x-ray diffraction topography, with a spatial resolution set by the size of the focused beam [12]. The photon intensity incident in the micro-focused spot was roughly 5×10^9/s, and the weakness of the CDW superlattice reflections limited counting statistics in feasible data collection times.

Figure 2 shows images of the CDW's microdiffraction intensity in the $\boldsymbol{b}^*$-$\boldsymbol{c}^*$ plane (i.e., the large face of the crystal) for sample B at $T = 120$ K. For an applied electric field $E = 0$, the thicker region of the crystal (below the dotted line) shows larger average intensities than the thinner region (above the dotted line), as expected because of the difference in diffracting volume. Electric fields larger than the depinning threshold (E_T) determined by the thicker, more weakly pinned region produce a decrease in intensity in the thicker region due to rotation of the CDW wave vector. Initially, the width of the region with reduced intensity increases with electric field, but it then saturates at large fields where both thick and thin regions

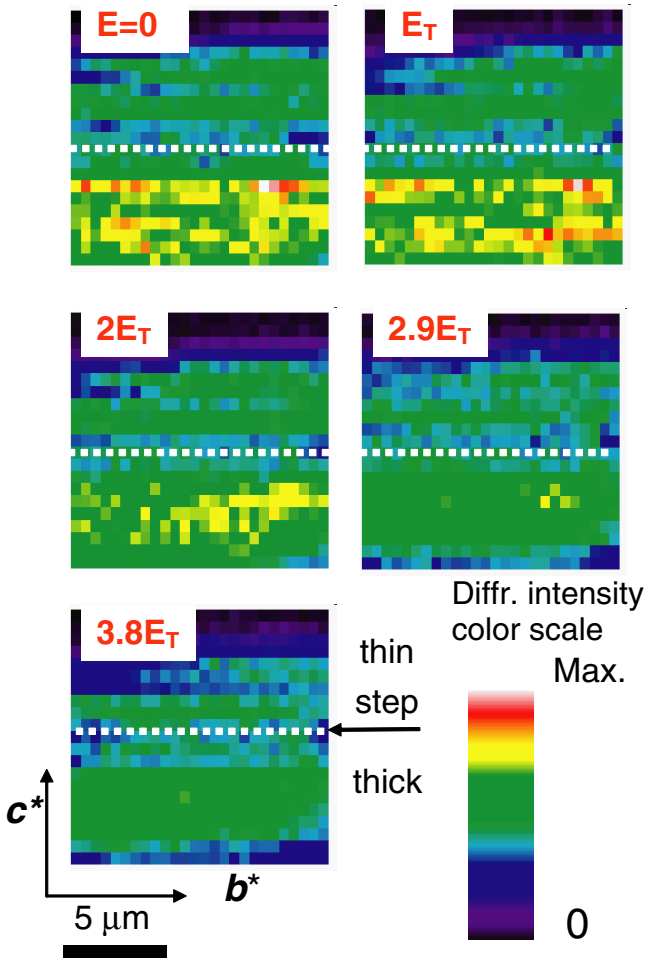

FIG. 2 (color online). Micro-beam diffraction intensity images at several electric fields for sample B at $T = 120$ K. The position of the thickness step is indicated by the horizontal dotted line.

are depinned. Similar behavior has been observed using x-ray topography [8] but with a spatial resolution of ~4 μm compared with less than 0.4 μm obtained here. One complication in these experiments was differential thermal contraction of the crystal, polymer, and substrate, which produced slight longitudinal (and smaller transverse) crystal deformations causing background intensity variations visible in images of both the CDW and main Bragg peak. Images of the Bragg peak similar to those in Fig. 2 were used to select flat regions for further study.

Previous work [7–9] has demonstrated that CDW shearing results from differences in pinning strength in thick and thin portions of the crystal. Shear along the thickness step should produce rotations of the CDW wave vector. Looking normal to the $\boldsymbol{b}^*$-$\boldsymbol{c}^*$ plane, CDW phase fronts in the thick region will be held back near the step by friction with the thin region, and phase fronts in the thin region will be pulled forward. The CDW wave vector (pointing normal to the phase fronts) will thus be tilted in the $\boldsymbol{b}^*$-$\boldsymbol{c}^*$ plane by an angle θ that is largest near the step and decreases away from it. Looking normal to the $\boldsymbol{a}^*$-$\boldsymbol{b}^*$ plane, the portion of

the thick region that rises above the top of the thin region is held back by the lower part of the thick region (which directly experiences friction with the thin region). The CDW wave vector in the thick region will thus also be tilted in the $\boldsymbol{a}^*$-$\boldsymbol{b}^*$ plane by an angle φ, with a maximum value near the step. Both of these rotation components will vary with position within the cross section, and this will produce peak broadening when the crystal is rocked about the angles θ and φ.

To examine the shearing process more closely, microdiffraction data was thus recorded versus bias and position while rocking the crystal about the angle φ. Figure 3 shows plots of the diffracted intensity versus angle φ at several positions y along the $\boldsymbol{c}^*$ direction for three different applied electric fields $E > E_T$, measured at $T = 90$ K. Of many rocking curves recorded, we show a pair close to the step (circles and triangles) and a pair (diamonds and stars) far away from the step. The diffraction profiles near the step show significant changes in both shape and the center position, in contrast to the curves acquired far from the step, which are not changed by the electric field. Moving across the sample's width, the center of the rocking curves shifts by up to 40 mdeg, depending on the electric field. The magnitude of this shift shows a maximum just above threshold; at large fields where the CDW in both the thick and thin parts of the cross section are depinned, the shift is smaller and the peaks are broadened. No such position-dependent shifts in peak position were observed in the zero-field-cooled state for $E < E_T$, although significant CDW distortions could be frozen in when the CDW was repinned.

Figure 4(a) shows an alternative representation of the data, plotting the rotation of the CDW's wave vector (shift of the peak position in φ) as a function position y along $\boldsymbol{c}^*$,

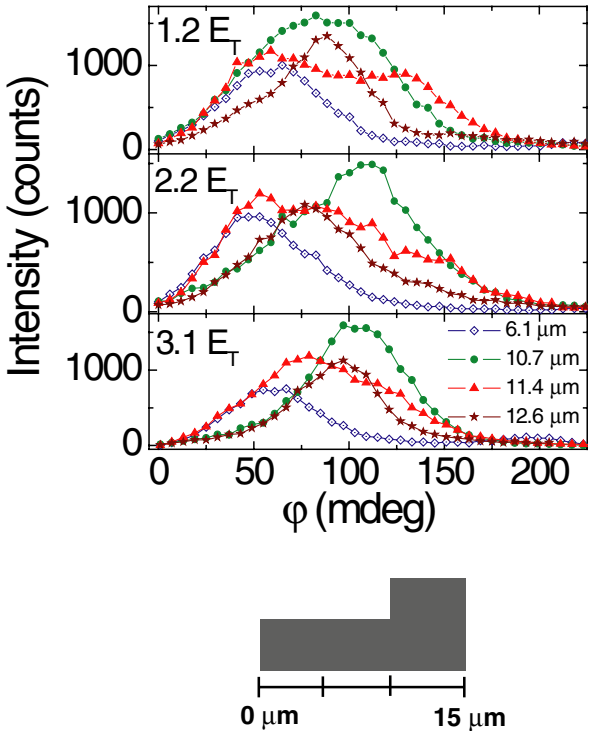

FIG. 3 (color online). Rocking curves of intensity vs angle φ at positions on either side of the thickness step of sample A, for three different electric fields at $T = 90$ K.

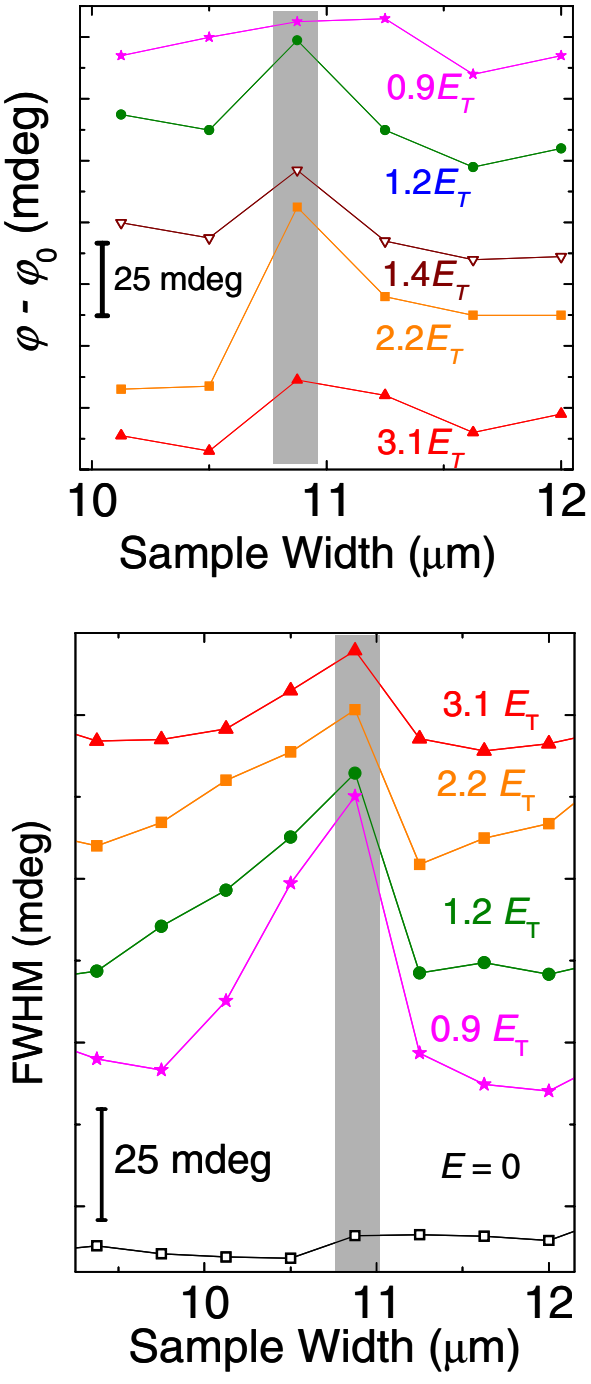

FIG. 4 (color online). CDW $\boldsymbol{q}$-vector rotation (upper panel) and rocking peak full width at half maximum (lower panel) vs position near the thickness step for sample A, for several electric fields at $T = 90$ K. Curves are vertically offset for clarity.

for several electric fields. These data clearly show that the shift φ has a maximum near the step position, and that this shift decreases at large fields. The region of large rotations is confined to within roughly 1 μm of the step, and shear strains have nearly fully relaxed 3 μm away from the step. The nearly symmetric variation of φ across the step is likely due to the relatively small variation in pinning strength across the step. This allows deformations to extend well into the thinner, more strongly pinned region even when the CDW there remains stationary. Figure 4(b) shows the corresponding variation of the full width at half maximum (FWHM) of the peak in φ versus position y, for the same range of electric fields. Both the wave vector rotation φ and the FWHM of the intensity variation with φ show maxima in the vicinity of the step. This latter fact is most likely connected to the sample geometry and the variable mixing of φ and θ rotations within the volume illuminated by the x-ray micro-beam.

Although clear wave vector rotations are observed near the step in crystal thickness, no rotations are observed near the edges of the crystal. This rules out strong CDW pinning by crystal surfaces, which would be expected to produce wave vector rotations increasing from zero near the crystal center to maxima at its (strongly pinned) surfaces [2].

For both crystals studied, the maximum magnitude of the CDW wave vector rotation at the step was approximately 0.03°, corresponding to a maximum CDW shear strain of $\varepsilon_s \sim 5 \times 10^{-4}$. This compares with a longitudinal strain $\varepsilon \sim 1.3 \times 10^{-3}$ measured at $T = 90$ K in $NbSe_3$ at comparable electric fields $E > E_T$ [14]. These shear-induced wave vector rotations explain the field-dependent transverse peak broadenings observed in previous x-ray diffraction studies of $NbSe_3$.

O'Neill *et al.* [10] determined the shear strength of the CDW in $NbSe_3$ from transport measurements on samples with microfabricated steps. At $T = 120$ K, the measured plastic shear strength was $\sigma_s = 9.5 \times 10^3$ N/m^2, roughly 30 times smaller than the longitudinal shear stress at which substantial CDW phase slip is observed [14]. Taking the ratio of this shear stress to the maximum shear strain yields an estimate for the CDW's shear modulus of $G = 1.8 \times 10^7$ N/m^2. This is roughly 50 times smaller than the CDW's measured longitudinal modulus [14], consistent with $NbSe_3$'s electronic anisotropy [15]. Torsional resonance measurements [16] yield a fractional change in the shear modulus of $NbSe_3$ crystals upon CDW depinning $\Delta G = (G(E > E_T) - G_0)/G_0$ of $\sim 10^{-3}$, consistent with our measurements and estimates of the CDW's contribution to the crystal's shear modulus. Neutron scattering measurements [17] of acoustic phason velocities in the CDW conductor $K_{0.3}MoO_3$ give transverse-to-longitudinal ($\boldsymbol{b}^*$) velocity ratios of 0.1 and 0.44 for the $2\boldsymbol{a}^* - \boldsymbol{c}^*$ and $2\boldsymbol{a}^* + \boldsymbol{c}^*$ directions, respectively, corresponding to shear-to-longitudinal moduli ratios of 0.01 and 0.2. These are comparable to the value found here.

In conclusion, x-ray micro-beam diffraction has allowed direct measurement of CDW shear strain profiles and an estimate of the CDW's shear modulus. It should prove to be a powerful probe of plasticity in moving CDWs and related electronic crystals.

We acknowledge discussions with Eric Isaacs in the early stages of this project. This work was supported by the NSF (DMR 04-05500). The Advanced Photon Source is supported by the U. S. Department of Energy, Office of Science, Office of Basic Energy Sciences, under Contract No. W-31-109-Eng-38. Sample mounts were prepared using the Cornell Nanoscale Facility, a member of the National Nanotechnology Infrastructure Network, which is supported by the National Science Foundation (Grant No. ECS 03-35765).

*Electronic mail: ret6@cornell.edu
†Now at NIST, Boulder, CO, USA.

[1] J. P. Pouget, *Structural and Dynamical Aspects of the Charge Density Wave Instability, in Physics and Chemistry of Low-Dimensional Inorganic Conductors*, edited by C. Schlenker, M. Greenblat, J. Dumas, and S. van Smaalen, NATO-ASI Vol. 254 (Plenum, New York, 1996).
[2] D. Feinberg and J. Friedel, in *Low-Dimensional Electronic Properties of Molybdenum Bronzes and Oxides*, edited by C. Schlenker (Kluwer Academic, Dordrecht, 1989), p. 407.
[3] G. Gruner, *Density Waves in Solids* (Addison-Wesley, Reading, MA, 1994).
[4] C.-H. Du *et al.*, Phys. Rev. Lett. **84**, 3911 (2000); U. Yaron *et al.*, Nature (London) **376**, 753 (1995).
[5] E. Y. Andrei *et al.*, Phys. Rev. Lett. **60**, 2765 (1988).
[6] G. Blatter *et al.*, Rev. Mod. Phys. **66**, 1125 (1994); S. Yoon *et al.*, Science **255**, 165 (1992).
[7] J. McCarten *et al.*, Phys. Rev. B **46**, 4456 (1992).
[8] Y. Li *et al.*, Phys. Rev. Lett. **83**, 3514 (1999).
[9] M. P. Maher *et al.*, Phys. Rev. B **43**, 9968 (1991).
[10] K. O'Neill, K. Cicak, and R. E. Thorne, Phys. Rev. Lett. **93**, 066601 (2004).
[11] P. G. Evans *et al.*, Science **295**, 1042 (2002).
[12] Yeong-Ah Soh *et al.*, J. Appl. Phys. **91**, 7742 (2002).
[13] Z. Cai, B. Lai, Y. Xiao, and S. Xu, J. Phys. IV **104**, 17.
[14] D. DiCarlo *et al.*, Phys. Rev. Lett. **70**, 845 (1993); T. L. Adelman *et al.*, Phys. Rev. B **53**, 1833 (1996); H. Requardt *et al.*, Phys. Rev. Lett. **80**, 5631 (1998).
[15] N. P. Ong and J. W. Brill, Phys. Rev. B **18**, 5265 (1978); E. Slot and H. S. J. van der Zant, J. Phys. IV **12**, 103 (2002).
[16] X.-D. Xiang and J. W. Brill, Phys. Rev. B **39**, 1290 (1989).
[17] B. Hennion, J. P. Pouget, and M. Sato, Phys. Rev. Lett. **68**, 2374 (1992).